

# Detectable Signatures of Cosmic Radiative Feedback

R. Schneider<sup>1\*</sup>, R. Salvaterra<sup>2</sup>, T. Roy Choudhury<sup>3</sup>, A. Ferrara<sup>4</sup>, C. Burigana<sup>5</sup>  
and L. A. Popa<sup>5,6</sup>

<sup>1</sup> *INAF - Osservatorio Astrofisico di Arcetri, Largo Enrico Fermi 5, 50125 Firenze, Italy*

<sup>2</sup> *Dipartimento di Fisica G. Occhialini, Università degli Studi di Milano Bicocca, Piazza della Scienza 3, I-20126 Milano, Italy*

<sup>3</sup> *Institute of Astronomy, Madingley Road, Cambridge CB3 0HA, UK*

<sup>4</sup> *SISSA/International School for Advanced Studies, Via Beirut 4, 34100 Trieste, Italy*

<sup>5</sup> *INAF-IASF Bologna, via Gobetti 101, I-40129 Bologna - Italy*

<sup>6</sup> *Institute for Space Sciences, Bucharest-Magurele, Str. Atomostilor, 409, PoBox Mg-23, Ro-077125, Romania*

28 November 2007

## ABSTRACT

We use a semi-analytical model to study the impact of reionization, and the associated radiative feedback, on galaxy formation. Two feedback models have been considered: (i) a standard prescription, according to which star formation is totally suppressed in galaxies with circular velocity below a critical threshold (model CF06) and (ii) a characterization based on the filtering scale (model G00), allowing for a gradual reduction of the gas available for star formation in low-mass galaxies. In model CF06 reionization starts at  $z \lesssim 15-20$ , is 85% complete by  $z \sim 10$ ; at the same  $z$ , the ionized fraction is 16% in model G00. The models match SDSS constraints on the evolution of the neutral hydrogen fraction at  $z < 7$ , but predict different Thomson optical depths,  $\tau_e = 0.1017$  (CF06), and  $0.0631$  (G00); such values are within  $1\sigma$  of the *WMAP* 3-yr determination. Both models are in remarkable good agreement with additional existing data (evolution of Lyman-limit systems, cosmic star formation history, high- $z$  galaxy counts, IGM thermal history), which therefore cannot be used to discriminate among different feedback models. Deviations among radiative feedback prescriptions emerge when considering the expected HI 21 cm background signal, where a  $\sim 15$  mK absorption feature in the range 75-100 MHz is present in model G00 and a global shift of the emission feature preceding reionization towards larger frequencies occurs in the same model. Single dish observations with existing or forthcoming low-frequency radio telescopes can achieve mK sensitivity, allowing the identification of these features provided that foregrounds can be accurately subtracted.

**Key words:** Cosmology: theory - galaxies: formation - intergalactic medium - diffuse radiation

## 1 INTRODUCTION

The process of cosmic reionization is of primary importance in the evolution of the Universe. Reionization is a consequence of the formation of the first luminous sources that shine after the Dark Ages, but it also has a dramatic impact on subsequent galaxy evolution. Despite the recent progress in observational and theoretical studies, fundamental questions such as what are the dominant sources of reionization and how long did the process take still require complete and definite answers.

The latest analysis of Ly $\alpha$  absorption in the spectra of the 19 highest redshift Sloan Digital Sky Survey (SDSS) quasars (QSOs) shows a strong evolution of

the Gunn-Peterson Ly $\alpha$  opacity at  $z \sim 6$  (Fan et al. 2006; Gallerani, Choudhury & Ferrara 2006). This result, together with the downward revision of the electron scattering optical depth to  $\tau_e = 0.09 \pm 0.03$  in the release of the 3-yr *Wilkinson Microwave Anisotropy Probe* (*WMAP*) data (Page et al. 2007; Spergel et al. 2007), is consistent with “minimal reionization models” which do not require the presence of very massive ( $M > 100M_\odot$ ) Population III stars (Choudhury & Ferrara 2006; Gnedin & Fan 2006).

Choudhury & Ferrara (2005, 2006) have developed a self-consistent formalism which allows to jointly study cosmic reionization and the thermal history of the intergalactic medium (IGM). Their semi-analytic model accounts for inhomogeneous IGM density distribution, three different classes of ionizing photons (Population III, Population II stars and QSOs), and radiative feedback inhibiting star for-

\* raffa@arcetri.astro.it

mation in low-mass galaxies. Note that Population III (Pop III) stars in this model are characterized by a standard Salpeter Initial Mass Function (IMF) extending in the range  $1 - 100 M_{\odot}$ . The model free parameters are constrained by a wide range of observational data. From this analysis, it emerges that hydrogen reionization starts around  $z \approx 15$  driven by the contribution of Pop III stars and it is 80% complete by  $z \approx 10$ ; below this redshift, the contribution of Pop III stars decreases because of the combined action of radiative and chemical feedback. As a consequence, reionization is extended considerably, completing only at  $z \approx 6$  (Choudhury & Ferrara 2006).

These results are consistent with the study of Gnedin & Fan (2006), who used a set of numerical simulations with different spatial and mass resolutions to make a detailed comparison with SDSS and *WMAP* data. Assuming the sources of ionizing photons to be Population II (Pop II) stars and QSOs, they find that the simulations can match the SDSS observations in the range  $5 < z < 6.2$ , but do not have enough resolution to resolve the earliest stages of star formation. Depending on the fractional contribution of Pop III stars, the optical depth to Thomson scattering varies in the range  $0.06 < \tau_e < 0.10$ , consistent with the 3-yr *WMAP* results.

Since it appears that minimal reionization models provide the best theoretical frameworks for the existing data, we can use these models to explore the effects of reionization on galaxy formation, to which we will refer to as “radiative feedback”.

It is well known that the temperature increase of the cosmic gas in ionized regions leads to a dramatic suppression of the formation of low-mass galaxies. Such suppression has been found to become effective in dark matter halos with circular velocity below a critical one,  $v_{\text{crit}}$ , whose value is loosely constrained by a number of studies (Thoul & Weinberg 1996; Susa & Kitayama 2000; Kitayama et al. 2001; Machacek et al. 2001; Dijkstra et al. 2004). Values in the range  $v_{\text{crit}} = 10 - 50$  km/s are found, depending on the assumed intensity of the UV background, the inclusion of radiative transfer effects, the numerical scheme adopted, and the investigated redshift range (see Ciardi & Ferrara 2005 for an extensive review). This radiative feedback prescription is therefore unable to quantify the decrease in the amount of gas available for star formation in low-mass halos: it simply states that galaxies can form stars unimpeded provided that their halos have circular velocities  $> v_{\text{crit}}$ .

A perhaps more complete characterization of radiative feedback on low-mass galaxy has been obtained by Gnedin (2000). Based on cosmological simulations of reionization, this study shows that the effect of photoionization is controlled by a single mass scale in both the linear and non linear regimes. The gas fraction within dark matter halos at any given moment is fully specified by the current filtering mass, which directly corresponds to the length scale over which baryonic perturbations are smoothed in linear theory. The results of this study provide a quantitative description of radiative feedback, independently of whether this is physically associated to photoevaporative flows or due to accretion suppression.

In the present paper, we show that these two different feedback prescriptions have important effects on the

reionization history and on the properties of the sources which dominate the process. Using the semi-analytic model of Choudhury & Ferrara (2005, 2006), we compare the results obtained for these two competitive feedback models with a wide range of observational data, ranging from the redshift evolution of Lyman-limit absorption systems, the Gunn-Peterson and electron scattering optical depths, the cosmic star formation history, and number counts of high- $z$  sources in the NICMOS Hubble Ultra Deep Field (HUDF). We find that in spite of this demanding benchmark of observations, existing data are unable to discriminate among the two reionization histories. We therefore explore an alternative method to break these degeneracies using future 21 cm experiments such as the Low Frequency Array (LOFAR), the 21-Centimeter Array (21CMA), the Mileura Wide Field Array (MWA), and the Square Kilometer Array (SKA); these instruments are expected to reach the sensitivity required to perform accurate maps of the neutral hydrogen distribution from the Dark Ages to the latest stages of the reionization process.

The paper is organized as follows: in Section 2 we give a brief description of the semi-analytic formalism and present the results of the two radiative feedback models, comparing these with existing observations; in Section 3 we compute the predicted global 21 cm background in the two models and discuss its detectability with on-going and future facilities. Finally, Section 4 summarizes our conclusions.

Throughout this paper, we adopt a flat  $\Lambda$ CDM cosmological model consistent with 3-yr *WMAP* data (Spergel et al. 2007), with matter and cosmological constant density parameters  $\Omega_m = 0.24$  and  $\Omega_{\Lambda} = 0.76$ , reduced Hubble constant  $h = 0.73$ , baryon density  $\Omega_b h^2 = 0.022$ , density contrast  $\sigma_8 = 0.74$ , and adiabatic scalar perturbations (without running) with spectral index  $n_s = 0.95$ . We also assume a Cosmic Microwave Background (CMB) temperature of 2.725 K (Mather et al. 1999).

## 2 REIONIZATION MODELS

In this Section we first summarize the main features of the semi-analytical model developed by Choudhury & Ferrara (2005) with the additional physics introduced in Choudhury & Ferrara (2006). We then describe the two alternative radiative feedback prescriptions and compare the resulting reionization histories with existing data.

### 2.1 Model description

The main features of the formalism developed by Choudhury & Ferrara (2005, 2006) can be summarized as follows:

- **Inhomogeneous reionization:** the model accounts for IGM inhomogeneities by adopting the procedure of Miralda-Escudé, Haehnelt & Rees (2000). The overdensity distribution is assumed to be lognormal. The distribution determines the mean free path of photons,

$$\lambda_{\text{mfp}}(z) = \frac{\lambda_0}{[1 - F_V(z)]^{2/3}} \quad (1)$$

where  $F_V$  is the volume fraction of ionized regions and  $\lambda_0$

**Table 1.** Best-fit parameters for models CF06 and G00 shown in Figs. 2 and 3. For the same models, we also report the residual volume-averaged neutral hydrogen fraction at redshift 6,  $x_{\text{HI}}(6)$ , the volume-averaged electron fraction at redshift 10,  $x_e(10)$ , and the Thomson scattering optical depth  $\tau_{\text{el}}$  (see text).

Model	$\epsilon_{*,\text{II}}$	$f_{\text{esc},\text{II}}$	$\epsilon_{*,\text{III}}$	$f_{\text{esc},\text{III}}$	$x_{\text{HI}}(6)$	$x_e(10)$	$\tau_{\text{el}}$
CF06	0.10	0.01	0.03	0.68	$4 \times 10^{-4}$	0.85	0.1017
G00	0.10	0.01	0.01	0.12	$3.9 \times 10^{-4}$	0.16	0.0631

is a normalization constant fixed by comparing with low-redshift observations of Lyman-limit systems.

- Sources of ionizing photons: the IGM is treated as a multiphase medium, following the thermal and ionization histories of neutral, HII, and HeIII regions simultaneously. Three sources have been assumed to contribute to the ionizing flux: (i) Pop III stars, assumed to be distributed according to a standard Salpeter IMF, as suggested by the combination of constraints from source counts at  $z \sim 10$  and *WMAP* data (Schneider et al. 2006); (ii) Pop II stars, with  $Z = 0.2Z_{\odot}$  and Salpeter IMF; (iii) QSOs which are significant sources of hard photons at  $z \lesssim 6$ . The emission is modelled using the stellar population synthesis templates from Bruzual & Charlot (2003) for Pop II stars and from Schaerer (2002) for Pop III stars.

- Chemical feedback: the transition from Pop III to Pop II stars is controlled by chemical feedback and occurs over a prolonged epoch rather than at a precise transition redshift. Using the merger-tree model developed by Schneider et al. (2006), at each redshift we classify star forming halos as hosting Pop II (Pop III) stars depending on whether the halo itself or any of its progenitors have (have not) already experienced an episode of star formation<sup>1</sup>. The fraction of Pop III halos decreases with time, being  $\approx 0.4, 0.32$ , and  $0.23$  at  $z = 15, 10$ , and  $5$ , respectively. At each redshift, Pop III stars are confined to form in halos with masses  $10^8 - 10^9 M_{\odot}$  which are large enough to form stars but small enough to be relatively unpolluted by their progenitors.

- Escape fractions: to reduce the number of model free parameters, Choudhury & Ferrara (2006) use a physical argument to relate the escape fractions of Pop III and Pop II ionizing photons. These scale according to the number of ionizing photons produced and depend on a single free-parameter,  $N_{\text{abs}}$ , which represents the number of ionizing photons absorbed within a star-forming halo, through the relation

$$\eta_{\text{esc}} \equiv \frac{N_{\text{abs}}}{\epsilon_{*,\text{II}} N_{\gamma,\text{II}}}. \quad (2)$$

The escape fractions for Pop II and Pop III stars are then given by the following expressions,

$$f_{\text{esc},\text{II}} = 1 - \text{Min}[1, \eta_{\text{esc}}] \quad (3)$$

$$f_{\text{esc},\text{III}} = 1 - \text{Min} \left[ 1, \frac{\epsilon_{*,\text{II}} N_{\gamma,\text{II}}}{\epsilon_{*,\text{III}} N_{\gamma,\text{III}}} \eta_{\text{esc}} \right]; \quad (4)$$

<sup>1</sup> Since Pop III stars are assumed to be distributed according to a Salpeter IMF, star formation in Pop III halos always leads to metal-enrichment as a consequence of type-II supernova explosions. This is equivalent to the strong feedback case,  $f_{\text{sn}} = 1$ , in the formalism of Schneider et al. (2006).

where  $N_{\gamma,\text{II}}$  ( $N_{\gamma,\text{III}}$ ) are the number of photons produced by Pop II (Pop III) stars per unit mass of stars formed, and  $\epsilon_{*,\text{II}}$  ( $\epsilon_{*,\text{III}}$ ) are the Pop II (Pop III) star formation efficiencies.

Further details on the models can be found in the original papers (Choudhury & Ferrara 2005, 2006).

## 2.2 Radiative feedback

A variety of feedback mechanisms can suppress star formation in mini-halos, i.e. halos with virial temperatures  $< 10^4$  K, particularly if their clustering is taken into account (Kramer et al. 2006). We therefore assume that stars can form in halos down to a virial temperature of  $10^4$  K, consistent with the interpretation of the 3-yr *WMAP* data (Haiman & Bryan 2006; but see also Alvarez et al. 2006). We then assume that these halos can be affected by radiative feedback according to two alternative prescriptions:

(i) Following Choudhury & Ferrara (2006), we assume that in photoionized regions halos can form stars *only* if their circular velocity exceeds the critical value

$$v_{\text{crit}} = \frac{2k_B T}{\mu m_p}, \quad (5)$$

where  $\mu$  is the mean molecular weight,  $m_p$  is the proton mass, and  $T$  is the average temperature of ionized regions, which we can compute self-consistently from the multiphase IGM model. Typically, for a temperature of  $3 \times 10^4$  K, the minimum circular velocity is  $\approx 30$  km/s, within the range of values found in the literature (see Section 1 and Ciardi & Ferrara 2005 for a complete reference list). Note that the above value for  $v_{\text{crit}}$  evolves according to the gas temperature and it is not fixed to a particular value. Hereafter, we shall refer to this model as CF06.

(ii) Following Gnedin (2000), we assume that the average baryonic mass  $M_b$  within halos in photoionized regions is a fraction of the universal value  $f_b = \Omega_b/\Omega_m$ , given by the following fitting formula,

$$\frac{M_b}{M} = \frac{f_b}{[1 + (2^{1/3} - 1)M_C/M]^3}, \quad (6)$$

where  $M$  is the total halo mass, and  $M_C$  is the total mass of halos that on average retain 50% of their gas mass. A good approximation for the characteristic mass  $M_C$  is given by the linear-theory filtering mass,

$$M_{\text{F}}^{2/3} = \frac{3}{a} \int_0^a da' M_{\text{J}}^{2/3}(a') \left[ 1 - \left( \frac{a'}{a} \right)^{1/2} \right], \quad (7)$$

where  $a$  is the cosmic scale factor,

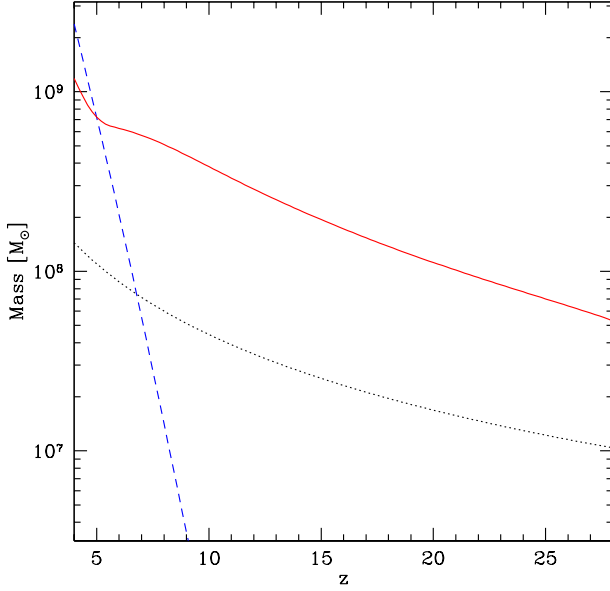


**Figure 1.** Redshift evolution of the filtering mass for the G00 model (dashed line), the minimum mass of star forming halos (dotted line), and the critical mass in ionized regions for the CF06 model (solid line).

$$M_J \equiv \frac{4\pi}{3} \bar{\rho} \left( \frac{\pi c_s^2}{G \bar{\rho}} \right)^{3/2},$$

is the Jeans mass,  $\bar{\rho}$  is the average total mass density of the Universe, and  $c_s$  is the gas sound speed. Since the gas density and temperature are not uniform, the sound speed is computed according to

$$c_s^2 = \frac{5}{3} \frac{k_B \langle T \rangle_V}{\mu m_p},$$

where  $\langle T \rangle_V$  indicates the volume-averaged gas temperature (Gnedin 2000). Hereafter, we will refer to this model as G00.

In Fig. 1 the filtering mass for the G00 model (dashed line) and the critical mass in ionized regions for the CF06 model (solid line) are plotted as a function of redshift. While these masses play different roles in the two feedback models, it is interesting to compare them with the minimum halo mass allowed to form stars (dotted line).

### 2.3 Results

The semi-analytical model depends only on four free parameters: the star formation efficiencies of Pop II and Pop III stars, the parameter  $\eta_{\text{esc}}$  which is related to the escape fraction of ionizing photons emitted by Pop II and Pop III stars (see equation 2), and the normalization of the photon mean free path,  $\lambda_0$  (see equation 1), which is fixed to reproduce low-redshift observations of Lyman-limit systems (Choudhury & Ferrara 2005). In Figs. 2 and 3 we show how the two models compare to existing observational data. The best-fitting parameters for each model are reported in Table 1. Both models show a remarkable agreement with a variety of observations. However, the two feedback prescriptions

have a noticeable impact on the overall reionization history and the relative contribution of different ionizing sources. The main reason is that, although the two models predict similar global star formation histories dominated by Pop II stars (panels b), the Pop III star formation rates have markedly different redshift evolution. In fact, chemical feedback forces Pop III stars to live preferentially in the smallest, quasi-unpolluted halos (virial temperature  $\gtrsim 10^4$  K), which are those most affected by radiative feedback (see Figure 1).

In model CF06, where star formation is totally suppressed below  $v_{\text{crit}}$ , Pop III stars disappear at  $z \sim 6$ ; conversely, in model G00, where halos suffer a gradual reduction of the available gas mass, Pop III stars continue to form at  $z \lesssim 6$ , though with a declining rate. As the star formation and photoionization rate at these redshifts are well constrained by observations, the star formation efficiency and escape fraction of Pop III stars need to be lower in model G00 in order to match the data (see Table 1). Because of this low  $f_{\text{esc,III}} \times \epsilon_{*,\text{III}}$ , reionization starts late in model G00 ( $z \lesssim 15$ ) and only 16% of the volume is reionized at  $z = 10$  (reionization starts at  $z \sim 20$  in model CF06 and it is 85% complete by  $z = 10$ ). For  $6 < z < 7$ , QSOs, Pop II and Pop III give a comparable contribution to the total photo-ionization rate in model G00, whereas in model CF06 reionization at  $z < 7$  is driven primarily by QSOs, with a smaller contribution from Pop II stars only. The predicted electron scattering optical depths are consistent with *WMAP* 3-yr data but with  $\sim 1\sigma$  difference among the two models, leaving a chance of probing them with forthcoming CMB experiments. Of course, it would still be interesting to see whether we can find any additional detectable signatures, particularly with respect to the upcoming 21cm experiments, which is discussed in the next section.

### 3 21 CM SIGNAL

The predicted free electron fraction and gas temperature evolution in the redshift range  $7 < z < 20$  represent the largest difference among the two feedback models. Therefore, the global 21 cm signal emitted during these cosmic epochs might provide a viable tool to discriminate the two scenarios.

The 21 cm brightness temperature, relative to the CMB, is given by

$$\begin{aligned} \delta T_b &= 27 x_{\text{HI}} (1 + \delta) \left( \frac{\Omega_b h^2}{0.023} \right) \left( \frac{0.15}{\Omega_m h^2} \frac{1+z}{10} \right)^{1/2} \\ &\times \left( \frac{T_S - T_\gamma}{T_S} \right) \text{mK}, \end{aligned} \quad (8)$$

where  $\delta$  is the fractional overdensity,  $x_{\text{HI}}$  is the hydrogen neutral fraction, and  $T_\gamma$  is the CMB temperature at redshift  $z$  (see Furlanetto, Oh & Briggs 2006 for a thorough review of the subject). The spin temperature  $T_S$ , which represents the excitation temperature of the 21 cm transition, determines whether the signal will appear in emission (if  $T_S > T_\gamma$ ) or in absorption (if  $T_S < T_\gamma$ ). The evolution of the spin temperature is controlled by three competitive processes: (i) absorption and stimulated emission of CMB photons, which tend to couple  $T_S$  to the CMB temperature; (ii) collisions

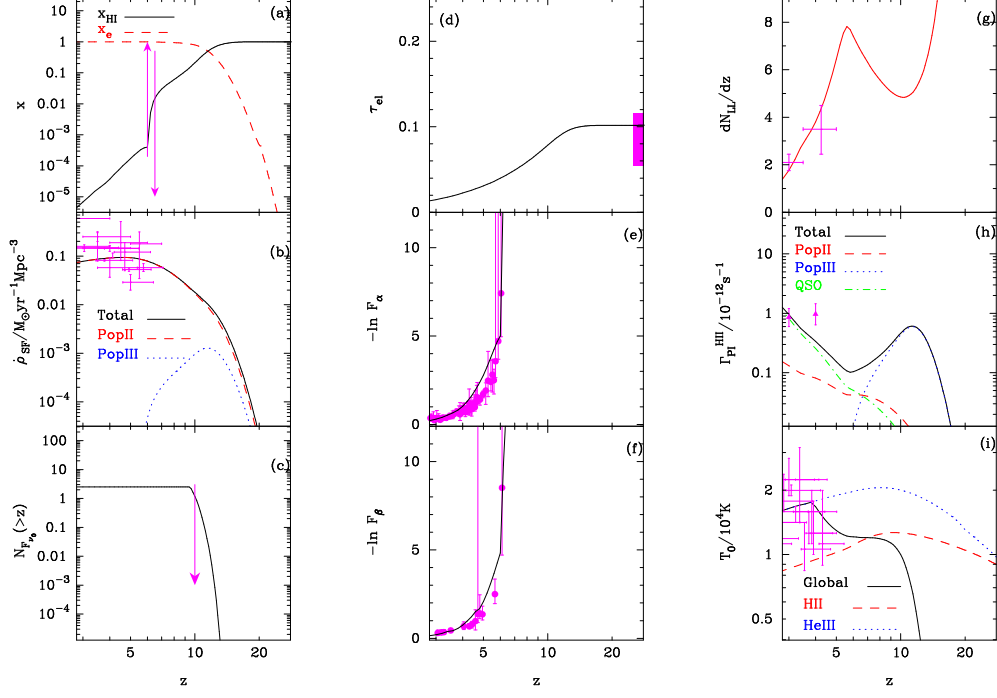


**Figure 2.** The best-fitting model CF06. The adopted parameters are given in Table 1. The panels show the redshift evolution of: (a) the volume-averaged electron and HI fraction. The arrows show an observational lower limit from QSO absorption lines at  $z = 6$  and upper limit from Ly $\alpha$  emitters at  $z = 6.5$ ; (b) the cosmic star formation history, with the contribution of Pop III and Pop II stars. Observational data are taken from the compilation of Nagamine et al. (2004); (c) the number of source counts above a given redshift, with the observational upper limit from NICMOS HUDF (Bouwens et al. 2005); (d) the electron scattering optical depth, with observational constraints from 3-yr *WMAP* data; (e) Ly $\alpha$  effective optical depth with data from Songaila (2004); (f) Ly $\beta$  effective optical depth with data from Songaila (2004); (g) the evolution of Lyman-limit systems with observational data from Storrie-Lombardi et al. (1994); (h) photoionization rates for neutral hydrogen, with estimates from numerical simulations (points with errorbars, Bolton et al. 2005); (i) temperature evolution of the mean density IGM, with observational data from Schaye (1999).

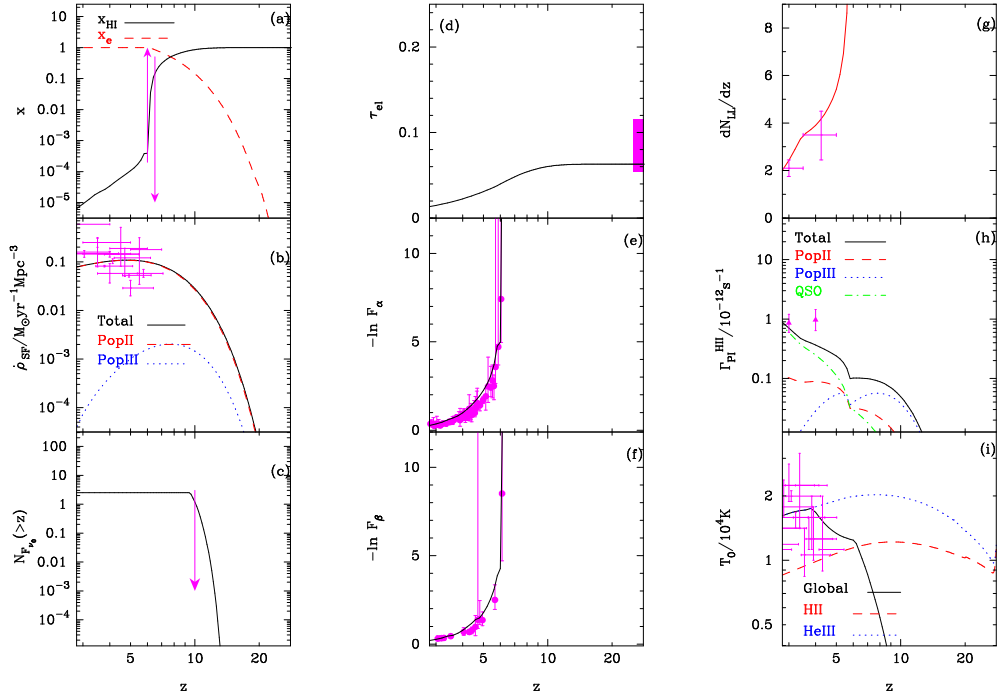


**Figure 3.** Same as Fig. 2 but for model G00. The adopted parameters are shown in Table 1.

with neutral hydrogen atoms and free electrons, which tend to couple  $T_S$  to the kinetic temperature of the gas  $T_K$ ; (iii) the absorption and subsequent spontaneous emission of  $\text{Ly}\alpha$  photons, which mix the hyperfine levels and couples  $T_S$  to an effective colour temperature  $T_C$  which, in most situations, can be well approximated by  $T_K$ . The latter process is referred to as Wouthuysen-Field (W-F) mechanism and it is effective in the presence of substantial UV light, requiring about 1  $\text{Ly}\alpha$  photon per baryon (Wouthuysen 1952; Field 1959). As a result, the spin temperature evolution can be written as

$$T_S^{-1} = \frac{T_\gamma^{-1} + x_C T_K^{-1} + x_\alpha T_C^{-1}}{1 + x_C + x_\alpha}, \quad (9)$$

where

$$x_C \equiv \frac{T_{21}}{T_\gamma} \frac{R_{21}^C}{A_{21}} \quad \text{and} \quad x_\alpha \equiv \frac{T_{21}}{T_\gamma} \frac{R_{21}^\alpha}{A_{21}}$$

are the coupling coefficients for collisions and UV scattering,  $T_{21} = 0.068$  K and  $A_{21} = 2.85 \times 10^{-15} \text{s}^{-1}$  are the equivalent temperature and spontaneous emission rate of the 21 cm transition, and  $R_{21}^C = n_H k_{21}^H + n_e k_{21}^e$  ( $R_{21}^\alpha$ ) is the rate coefficient for spin de-excitations by H-H and H-e collisions (UV scattering). In this analysis, we have used the value of  $k_{21}^H$  tabulated in Zygelman (2005)<sup>2</sup>, and the functional form of  $k_{21}^e(T_K)$  reported in Liszt (2001). The rate coefficient for the W-F mechanism is given by (Hirata 2006)

$$R_{21}^\alpha = \frac{8}{9} \pi \lambda_\alpha^2 \gamma S_\alpha J_\alpha,$$

where  $\lambda_\alpha = 1216$  Å,  $\gamma = 50 \text{ MHz}$  is the half width at half-maximum of the  $\text{Ly}\alpha$  resonance,  $J_\alpha$  is the flux of  $\text{Ly}\alpha$  photons (in  $\text{cm}^{-2} \text{s}^{-1} \text{Hz}^{-1} \text{sr}^{-1}$ ), and  $S_\alpha$  is a factor of order unity that accounts for spectral distortions. We have used the numerical fits of Hirata (2006) for  $S_\alpha$  and the effective colour temperature  $T_C$  which appears in equation (9).

Using equations (8) and (9), we can compute the all-sky 21 cm background signals predicted by the two radiative feedback models. We therefore take the redshift evolution of the gas kinetic temperature,  $T_K$ , and neutral hydrogen fraction,  $x_{\text{HI}}$ , for model CF06 and G00, shown respectively in panels (i) and (a) of Figs. 2 and 3. We compute the  $\text{Ly}\alpha$  background as

$$J_\alpha(z) = \frac{(1+z)^3}{4\pi} \int_z^\infty dz' \frac{dl}{dz'} \epsilon(\nu, z') e^{-\tau_{\text{eff}}(\nu_\alpha, z, z')},$$

where  $\nu = \nu_\alpha(1+z')/(1+z)$ ,  $dl/dz$  is the proper line element, and  $\tau_{\text{eff}}(\nu_\alpha, z, z')$  is the effective optical depth of the IGM to radiation emitted at  $z'$  and observed at  $z$  at frequency  $\nu_\alpha$  (see section 2.2 of Salvaterra & Ferrara 2003 for a full description of the IGM modelling). The comoving emissivity  $\epsilon(\nu, z)$  is computed as

$$\epsilon(\nu, z) = \int_z^\infty dz' l_\nu(t_{z,z'}) \dot{\rho}(z'),$$

<sup>2</sup> For kinetic temperatures in the interval  $1 \text{ K} < T_K < 300 \text{ K}$  we have used the recommended rates tabulated in column (4) of Table 2 and, for  $T > 300 \text{ K}$  we have applied the suggested analytic fit.

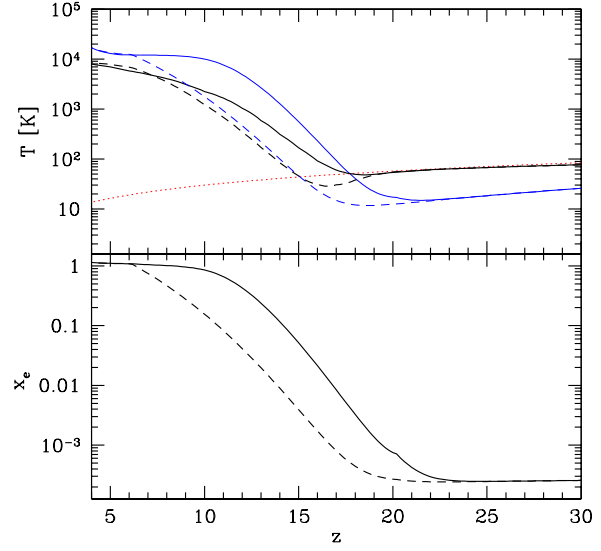


**Figure 4.** *Top panel:* redshift evolution of the spin (thick lines) and gas kinetic (thin lines) temperatures predicted by the two models. Solid lines refer to model CF06; dashed lines to model G00. For comparison, we also show the evolution of the CMB temperature (dotted line). *Bottom panel:* corresponding evolution of the free electron fraction.

where  $l_\nu(t_{z,z'})$  is the template specific luminosity for a stellar population of age  $t_{z,z'}$  (time elapsed between redshift  $z'$  and  $z$ ). The final value of  $\epsilon(\nu, z)$  is then computed by summing over the Pop II and Pop III contribution (Salvaterra et al. 2006). In Fig. 4 we show the evolution of the spin temperature, gas kinetic temperature and CMB temperature for the two models. As expected, at very high redshifts the spin temperature is coupled to the CMB, because collisions are negligible, and it decouples from the CMB because of the W-F effect, which determines the evolution at  $z \lesssim 20$ . As the star formation rate is dominated by Pop II stars, the  $\text{Ly}\alpha$  background is essentially maintained by Pop II stars at all redshifts, and it is almost independent of the small halos hosting Pop III stars, which are heavily affected by radiative feedback. As a consequence, the spin temperature is driven towards the corresponding color (kinetic) temperature with comparable rates in the two models; the different behavior in the redshift range  $7 \lesssim z \lesssim 19$  is all due to the dissimilar color (kinetic) temperature evolution caused by the two radiative feedback models. In particular, in model G00 the gas kinetic temperature is heated above the CMB value only at  $z \lesssim 15$ . Therefore, between  $15 \lesssim z \lesssim 20$ ,  $T_S < T_\gamma$  and we expect to see an absorption feature in the 21 cm signal which should be almost negligible in model CF06. Note that X-rays from supernovae, X-ray binaries and mini-QSOs can be an important heating agent for the neutral IGM. To cancel the predicted absorption feature, X-ray heating should increase the kinetic temperature from  $\sim 10$  K to values above  $\sim 30 - 40$  K in the redshift (time) interval  $17 < z < 20$  ( $\sim 50$  Myr). However, assuming that a fraction of 0.01 (0.1)

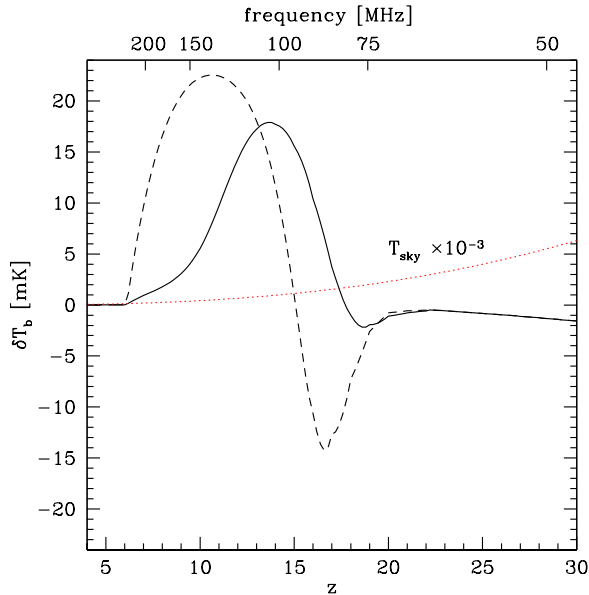


**Figure 5.** Predicted all-sky 21 cm brightness temperature relative to the CMB. Solid line refers to model CF06, dashed line to model G00. The upper x-axis shows a reference observational frequency scale. The dotted line shows an estimate of the foreground signal at these frequencies, rescaled by a factor  $10^{-3}$  (see text).

of the total energy at Ly $\alpha$  is emitted in X-rays (Chen & Miralda-Escudé 2004), the temperature evolution of neutral regions predicted by the CF06 and G00 models is found to deviate from adiabatic cooling only at  $z < 11$  ( $< 13$ ).

Fig. 5 shows the predicted 21 cm brightness temperature as a function of redshift. The upper x-axis shows some reference observational frequency values, computed as  $\nu = \nu_{21}/(1+z)$ , where  $\nu_{21} = 1420$  MHz. The expected absorption signal in model G00 appears in the frequency range 75 - 100 MHz and has an amplitude of  $\approx 15$  mK; this feature is far less evident in model CF06. At higher frequencies, the late reionization history predicted in model G00 (see the bottom panel of Fig. 4) causes a shift in the emission signal, which is larger than for model CF06. Note that since this is an all-sky signal, single-dish observations from existing and planned low-frequency radio-telescopes can reach the required mK sensitivity. The largest limitation to these measurements is the presence of strong foregrounds in the relevant frequency range. The dotted line is a naive estimate of the contamination of a quiet region of the sky from foregrounds (mainly Galactic synchrotron), taken from Furlanetto et al. (2006). It implies that the predicted signals should be completely screened by foregrounds, which are three orders of magnitude larger.

Since the frequency dependence of the signals and foregrounds are different, the gradient of the brightness fluctuation with frequency shows some spectral features that might help to discriminate the signal from the relatively smooth foreground. Fig. 6 shows the predicted gradient for the two models. The largest differences are due to the deeper absorption feature present in model G00, and to the shift of

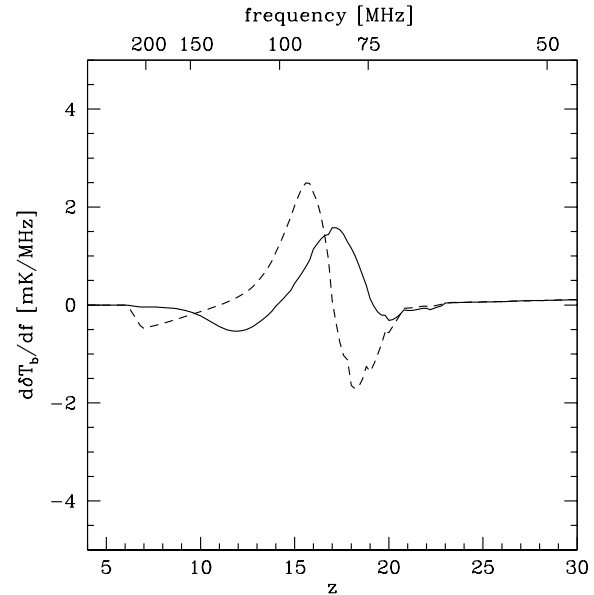


**Figure 6.** Frequency gradient of the 21 cm brightness shown in Fig. 5, adopting the same line coding.

the emission preceding reionization. Clearly, these are of order  $\approx 1 - 2$  mK/MHz and have to be extracted from a  $|dT_{\text{sky}}/d\nu| \gtrsim 3$  K/MHz foreground so that their detection will be very challenging. A discussion of possible strategies for this high-precision 21 cm measurement can be found in Furlanetto et al. (2006).

Following Valdes et al. (2007), we can tentatively assume that a successful detection requires the difference in the brightness temperature among the two models to be

$$\Delta \delta T_b = (\delta T_b)_{\text{G00}} - (\delta T_b)_{\text{CF06}} > 3 \text{ mK}$$

and the difference in the gradients to be,

$$\Delta \frac{d\delta T_b}{df} = \left( \frac{d\delta T_b}{df} \right)_{\text{G00}} - \left( \frac{d\delta T_b}{df} \right)_{\text{CF06}} > 0.6 \text{ mK/MHz}.$$

These conditions, based on the foreseen sensitivity of future 21 cm experiments, should take into consideration the difficulties associated with foregrounds removal. Using these limits as a guideline, Fig. 7 shows that the two radiative feedback models could be discriminated through the differences in their predicted 21 cm background signals in the observed frequency ranges 73-79 MHz and 82.5-97.2 MHz, which correspond to the redshift intervals 17-18.4 and 13.6-16.2, respectively.

## 4 CONCLUSIONS

Using a self-consistent semi-analytical model developed by Choudhury & Ferrara (2005) and recently updated by Choudhury & Ferrara (2006), we have explored the effect of reionization and its associated radiative feedback on galaxy formation. The suppression of star formation in low-mass galaxies due to the increase in temperature of the cosmic gas



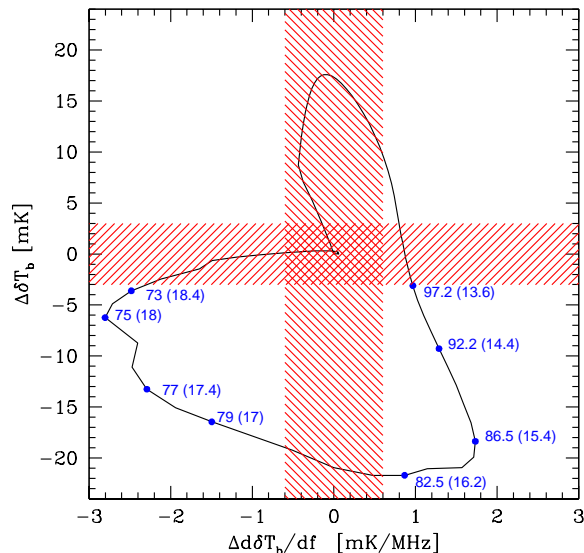


**Figure 7.** Difference in the brightness temperature and gradients between the two models (see text). The shaded areas represent the regions where the signals will not be distinguishable given the foreseen sensitivity of future 21 cm experiments. Numbers along the curves indicate the frequency in MHz (and the corresponding redshift) at which the signals would be observed.

in ionized regions has been modelled according to two different feedback prescriptions: (i) galaxies can form stars unimpeded provided that their circular velocity is larger than a critical threshold, which is not fixed to a constant value but evolves according to gas temperature (model CF06); (ii) depending on the mass of the galaxy, the fraction of gas available to star formation is reduced with respect to the universal value and it is fully specified by the filtering mass at that redshift (model G00). We then constrain the four free-parameters of each model with existing observational data, such as the redshift evolution of Lyman-limit absorption systems, the Gunn-Peterson and electron scattering optical depths, the cosmic star formation history, the number counts of high- $z$  sources in the NICMOS HUDF, and thermal history of the IGM. We find that:

(i) The two models provide equally good fit to existing observations, which therefore are not able to break the degeneracy among different radiative feedback implementations.

(ii) Given that Pop III stars are preferentially hosted in the smallest galaxies at each redshift, the largest difference between the two models reside in the predicted Pop III star formation history: in models CF06, Pop III stars are fully expired by  $z \sim 6$ , whereas in model G00 Pop III stars continue to form at lower  $z$ , though with decreasing rate.

(iii) The reionization and thermal history of the IGM are very different: reionization starts at  $z \lesssim 15 - 20$ , and it is already 85% complete by  $z \sim 10$  in model CF06, while, at the same  $z$ , the ionized fraction is only 16% in model G00. Both models match SDSS constraints on the evolution of the neutral hydrogen fraction at  $z < 7$ , but predict different

Thomson optical depth, with  $\tau_e = 0.1017, 0.0631$ , for model CF06 and G00, respectively, in agreement with *WMAP* 3-yr data. In principle, one can use this property to distinguish between the two models, particularly if the observed value of  $\tau_e$  is better constrained by future CMB experiments like PLANCK.

(iv) Given the different gas ionization fraction and temperature evolution in the range  $7 \lesssim z \lesssim 20$ , the two models predict different global 21 cm background signals in the observed frequency range  $75\text{MHz} \lesssim \nu \lesssim 200\text{ MHz}$ . The largest differences in the two models are represented by a  $\sim 15\text{ mK}$  absorption feature in the range 75-100 MHz in model G00 (which is nearly absent in model CF06), and by a global shift of the emission feature preceding reionization towards larger frequencies in the same model. Single dish observations with existing or forthcoming low-frequency radio telescopes such as LOFAR, 21CMA, MWA, and SKA can achieve mK sensitivity allowing the identification of these signals provided that foregrounds, which are expected to be three orders of magnitude larger, can be accurately subtracted.

(v) The best observational frequencies to discriminate the radiative feedback models through their 21 cm background signal are 73-79 MHz and 82.5-97.2 MHz, where the expected differences in brightness temperatures and gradients are large enough to be detectable with future 21 cm experiments.

How robust is the proposed method of differentiating the two radiative feedback models? It is important to stress that, for a given radiative feedback model, it is not possible to find a different set of parameters which provides an equally good fit to the data presented in figures 2 and 3 and yet produce a different 21cm signal. This is because the main difference between the G00 and CF06 models depends on (i) the confinement of Pop III stars in the smallest star forming halos by chemical feedback, and on (ii) how radiative feedback affects the gas content and therefore the star formation efficiency in these small mass objects. For the same reasons, we do not expect the resulting 21cm signals to be affected by varying star formation efficiencies and escape fractions with redshift and/or mass: at  $5 < z < 20$  more than 75% of Pop III halos are confined in a 0.5 dex mass bin centered on the minimum mass to form stars. Therefore we believe that the differences we predict in the 21cm signals are robust.

The absorption and emission features that we find are comparable to the 21 cm signatures expected in models which consider the high-redshift signals emerging from the Dark Ages, following the appearance of first luminous sources (Chen & Miralda-Escudé 2004; Sethi 2005; Furlanetto 2006), or induced by decaying/annihilating dark matter (Valdes et al. 2007). It is clear that measuring the 21 cm background would offer valuable insights into these early cosmic epochs. Our analysis suggests that self-consistent reionization models which are compatible with a large set of existing observational data predict different 21 cm background signals, which reflect how the process of star formation in the smallest galaxies is affected by radiative feedback. Future 21 cm data, complemented by the available observational data from SDSS, WMAP, thermal history of the IGM, high- $z$  number counts, and the cosmic star formation history, might break current degeneracies and constrain the



reionization process and its sources over the redshift range  $6 < z < 20$ .

## ACKNOWLEDGMENTS

We are grateful to Benedetta Ciardi for profitable discussions and to DAVID members<sup>3</sup> for fruitful comments. CB acknowledges the support by the ASI contract “Planck LFI Activity of Phase E2”.

## REFERENCES

- Alvarez, M. A., Shapiro, P. R., Ahn, K., Iliev, I. T. 2006, *ApJ*, 644, L101
- Bolton, J. S., Haehnelt, M. G., Viel, M., Springel, V. 2005, *MNRAS*, 357, 1178
- Bouwens, R. J., Illingworth, G. D., Thompson, R. I., Franx, M. 2005, *ApJ*, 624, L5
- Bruzual, G. & Charlot, S. 2003, *MNRAS*, 344, 1000
- Chen, X., Miralda-Escudé, J. 2004, *ApJ*, 602, 1
- Choudhury, T. R. & Ferrara, A. 2005, *MNRAS*, 361, 577
- Choudhury, T. R. & Ferrara, A. 2006, *MNRAS*, 371, L55 (CF06)
- Ciardi, B. & Ferrara, A. 2005, *Space Science Reviews*, 116, 625
- Dijkstra, M., Haiman, Z., Rees, M. J. 2004, *ApJ*, 601, 666
- Fan, X. et al. 2006, *AJ*, 132, 117
- Field, G. B., 1959, *ApJ*, 129, 536
- Furlanetto, S. R. 2006, *MNRAS*, 371, 867
- Furlanetto, S. R., Oh, P., Briggs, F. H., 2006, *Physics Reports*, 433, 4
- Gallerani, S., Choudhury, T. R. & Ferrara, A. 2006, *MNRAS*, 370, 1401
- Gnedin, N. 2000, *ApJ*, 542, 535 (G00)
- Gnedin, N. & Fan, X. 2006, *ApJ*, 648, 1
- Haiman, Z. & Bryan, G. L. 2006, *ApJ*, 650, 7
- Hirata, C. M. 2006, *MNRAS*, 367, 259
- Kitayama, T., Susa, H., Umemura, M., Ikeuchi, S. 2001, *MNRAS*, 326, 1353
- Kramer, R. H., Haiman, Z. & Oh, S. P. 2006, *ApJ*, 649, 570
- Liszt, H. 2001, *A&A*, 371, 698
- Machacek, M. M., Bryan, G. L., Abel, T. 2001, *ApJ*, 548, 509
- Mather, J. C., Fixsen, D. J., Shafer, R. A., Mosier, C., Wilkinson, D. T. 1999, *ApJ*, 512, 511
- Miralda-Escudé, J., Haehnelt M. & Rees, M. J., 2000, *ApJ*, 530, 1
- Nagamine, K., Cen, R., Hernquist, L., Ostriker, J., Springel, V., 2004, *ApJ*, 610, 45
- Page, L. et al. 2007, *ApJS*, 170, 335
- Salvaterra, R. & Ferrara, A., 2003, *MNRAS*, 339, 973
- Salvaterra R., Magliocchetti, M., Ferrara, A., Schneider, R., 2006, *MNRAS*, 368, L6
- Schaerer, D. 2002, *A&A*, 382, 28
- Schaye, J., Theuns, T., Leonard, A., Efstathiou, G. 1999, *MNRAS*, 310, 57
- Schneider, R., Salvaterra, R., Ferrara, A., Ciardi, B. 2006, *MNRAS*, 369, 825
- Sethi, S. 2005, *MNRAS*, 363, 818
- Songaila, A. 2004, *AJ*, 127, 2598
- Spergel, D. N. et al. 2007, *ApJS*, 170, 377
- Storrie-Lombardi, L. J., McMahon, R. G., Irwin, M. J. Hazard, C. 1994, *ApJ*, 427, L13
- Susa, H. & Kitayama, T. 2000, *MNRAS*, 317, 175
- Thoul, A. A. & Weinberg, D. H. 1996, *ApJ*, 465, 608
- Valdes, M., Ferrara, A., Mapelli, M., Ripamonti, E. 2007, *MNRAS*, 377, 245
- Wouthuysen, S. A., 1952, *AJ*, 57, 31
- Zygelman, B. 2005, *ApJ*, 622, 1356

<sup>3</sup> <http://www.arcetri.astro.it/science/cosmology>